11A.6

ON THE ROLE OF ATMOSPHERIC DATA ASSIMILATION AND MODEL RESOLUTION ON MODEL FORECAST ACCURACY FOR THE TORINO WINTER OLYMPICS

David R. Stauffer*[1], Glenn K. Hunter[1], Aijun Deng[1],
Jeffrey R. Zielonka[1], Karen Tinklepaugh[1],
Patrick Hayes[2] and Christopher Kiley[2]
[1] Pennsylvania State University, State College PA
[2] Northrop Grumman Corporation, Alexandria VA

1. INTRODUCTION

Local and regional scale atmospheric conditions strongly influence atmospheric transport and dispersion (AT&D) processes in the atmospheric boundary layer (ABL), and the extent and scope of the spread of dangerous materials in the lower levels of the atmosphere and in AT&D models (HPAC/SCIPUFF (Deng et al. 2004)). Managing the consequences of Chemical / Biological / Radiative / Nuclear (CBRN) incidents requires accurate current and future weather conditions to model potential effects (e.g., Stauffer et al. 2006). The role of continuous four-dimensional data assimilation (FDDA) and mesoscale model horizontal resolutions of 36 km, 12 km, 4 km and 1.3 km on meteorological (MET) accuracy and AT&D over varying terrain conditions and scales is investigated.

2. EXPERIMENTAL DESIGN

The accuracy of various MET inputs and their effect on HPAC predictions are investigated here over the varied and complex terrain of the Italian Alps and Torino Plains (Fig. 1). The ARPA-Piemonte special weather observations network (red dots in Fig. 1) available for the 2006 Winter Olympics period (10 – 27 February 2006) is used for model initialization and verification of the resulting 24-h forecasts. Mesoscale models are initialized with and without FDDA to determine its added value on MET accuracy. The FDDA experiments use either 1-sided or 2-sided temporal weighting of the observations. The latter (2-sided FDDA) is possible when the observations are already collected for the entire pre-forecast assimilation period before beginning the numerical forecast. The model can use observation nudging towards these data both before and after the observation time (Stauffer and Seaman 1994). The 1-sided FDDA experiments represent those realtime applications such as nowcasting when the model is continuously assimilating data as they become available (Schroeder et al. 2006). The observational data can thus only be used after the observation time with 1-sided temporal weights. The special observations are also used here for dynamic analysis where they are continuously assimilated within the mesoscale model throughout the 24-h periods to produce a more complete and dynamically consistent meteorological analysis than that provided by the observations alone.

**Corresponding author address:*
Dr. David R. Stauffer, 621 Walker Building, University Park, PA 16802; stauffer@meteo.psu.edu

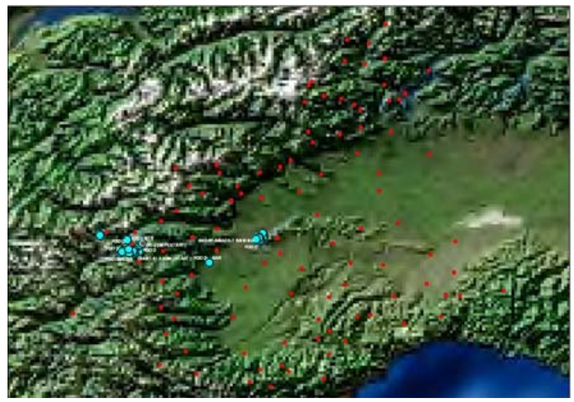

Figure 1. Locations of Winter Olympics venues (blue dots) and special ARPA-Piemonte mesonet data (red dots). Torino, Italy is located on the plain at the easternmost cluster of blue dots, and the Alps border the plain to the west and north.

This study also addresses the use of MET model data as HPAC/SCIPUFF inputs and whether the AT&D results warrant using these very fine meteorological model resolutions. HPAC predictions based on observations and dynamic analyses using the observations are compared against HPAC predictions using the various predictive weather model configurations for hypothetical releases and plume predictions in the mountains and on the plains. Some HPAC results will be presented at the conference.

3. METHODOLOGY

MM5 (Grell et al. 1995) high-resolution meteorological model forecasts are computed using a

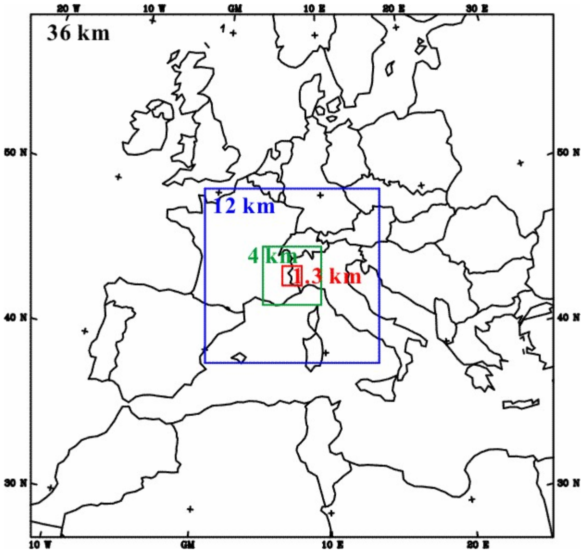

Figure 2. MM5 four-domain configuration for 2006 Winter Olympics cases.

2006 Torino Olympics Cases		
Case 1	00 UTC, 13 Feb - 00 UTC, 14 Feb	Dry
Case 2	12 UTC, 17 Feb– 12 UTC, 18 Feb	Precip/Wind in Mountains
Case 3	00 UTC, 18 Feb– 00 UTC, 19 Feb	Precip in Mountains
Case 4	12 UTC, 19 Feb– 12 UTC, 20 Feb	Precip in Mountains and on Plains
Case 5	00 UTC, 22 Feb– 00 UTC, 23 Feb	Precip on Plains
Case 6	12 UTC, 25 Feb– 12 UTC, 26 Feb	Light Precip in Mountains and on Plains

Table 1. Descriptions of the six case days used for this study.

42-CPU cluster running a four-nest configuration down to 1.3-km resolution over all the Olympics venues (Fig. 2). The case days chosen in Table 1 represent various combinations of dry, wet, misty or windy conditions in the mountains and/or plains. Statistics are computed for all model resolutions over the finest-resolution 1.3-km domain area using standard and the special Italian mesonet data. The importance of model resolution and the model initialization strategy for 24-h forecasts over this region of complex terrain will be explored.

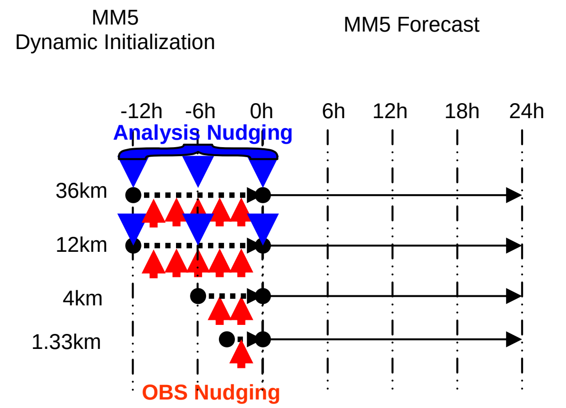

Figure 3. “Running start” model initialization FDDA strategy used for DTRA Olympics modeling support.

Model physics options were the same as those used in the MB2 baseline experiment in Deng and Stauffer (2006). A “running start” multiscale FDDA strategy (Stauffer and Seaman 1994) using a 3 – 12-h pre-forecast period assimilation of standard and special data over all four domains was used to improve model initialization and spinup during the subsequent 0 to 24-h forecasts (Fig. 3). This dynamic initialization allows model cloud and precipitation fields, and local circulations to be already spun up on the various scales at the initial time, which should produce improved forecasts of MET conditions for AT&D applications.

4. MET MODELING RESULTS

Some subjective analysis of the MM5 predictions as a function of model resolution will be presented first, followed by statistical results over the 1.3-km domain area for various model resolutions and model FDDA options.

The MM5 system predicted the very localized mountain flows in and around the Olympics venues when large-scale weather conditions were weak, and also the complex interactions of the terrain with the larger scale weather-producing systems when stormy conditions prevailed (Stauffer et al. 2006). Figure 4 shows an example of how model horizontal resolution affects the numerical prediction of downslope flow and channeled winds at the surface overlaid on top of the terrain field of each resolution domain. The narrow Alpine valleys containing highways leading to the mountain venues are well represented in the terrain of the 1.3-km terrain field, and are somewhat less resolved in the 4-km terrain field. Note the drainage flow coming out of one of these fingers towards the plain to the west of Torino. These local, terrain-forced flows are better-resolved at 1.3-km resolution, and better match the special

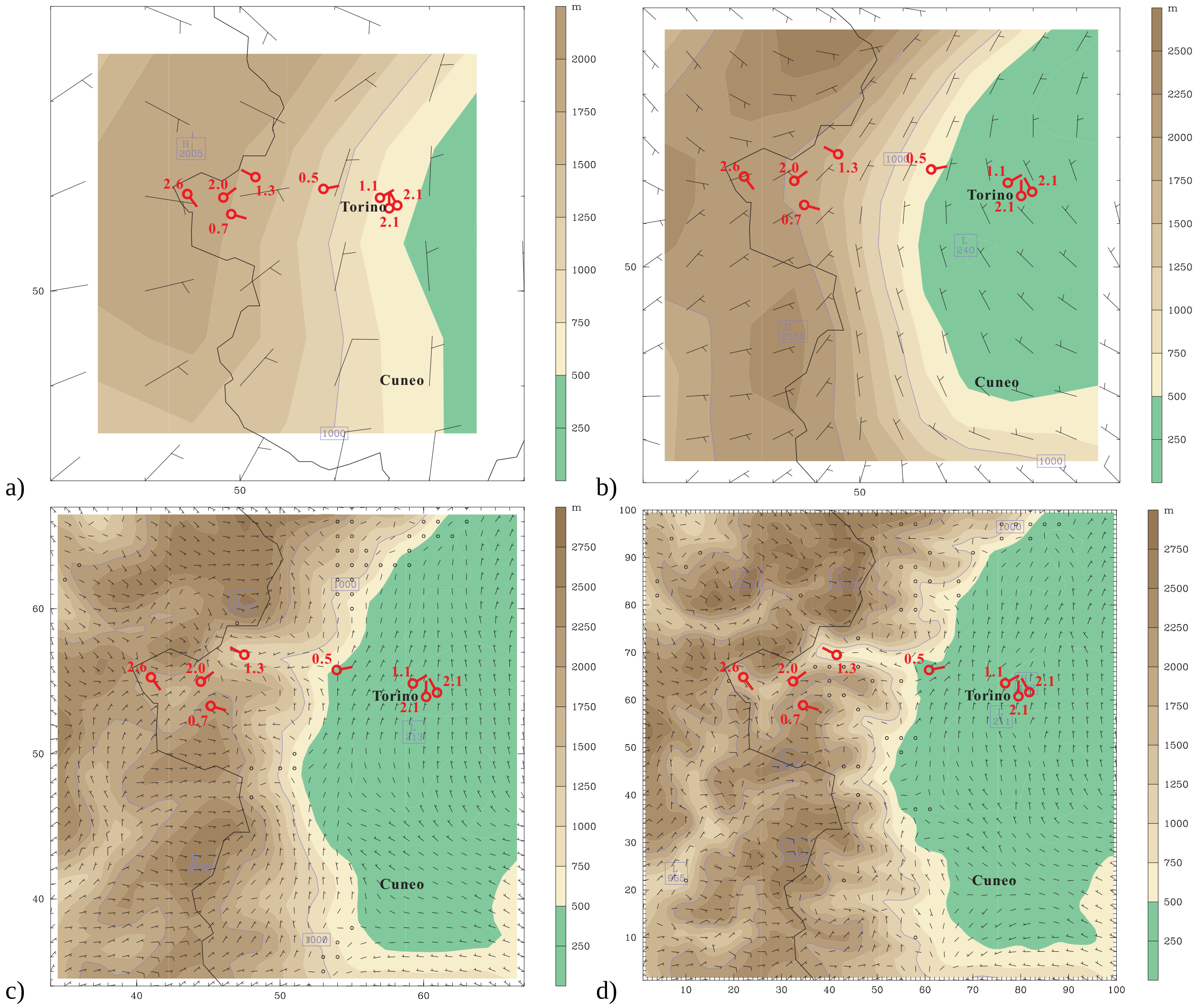

Figure 4. MM5 2-sided FDDA, 18-h surface wind prediction and observations at 18 UTC 21 February 2006 over the 1.3-km domain area for each model resolution forecast. Surface winds (ms^{-1}) are overlaid on the terrain field (m, color code on right of figure) for each model resolution domain. a) 36-km domain, b) 12-km domain, c) 4-km domain, d) 1.3-km domain. One full barb is 10 ms^{-1}. Dark line is France – Italy border.

observations compared to those based on coarser model resolutions of 4 km, and especially so compared to those at 12-km and 36-km resolutions. There are no fingers or valleys in the coarser resolution model terrain fields. In fact, Torino is in the mountains on the 36-km domain! These differences in the resolved meteorology fields may greatly affect the AT&D predictions in this region.

To analyze the role of model resolution on MET accuracy over this region, Fig. 5 shows the mean absolute error (MAE) of surface vector wind difference (VWD) averaged over the 24-h forecast period for each of the six case days at each model resolution. Note that for each case the 36-km domain has the largest surface wind errors compared to the mesonet observations, followed by those on the 12-km domain, and then those on the 4-km and 1.3-km domains. This is not surprising given the smoother terrain fields on the coarser model grids (Fig. 4). The finest two model resolutions of 1.3 km and 4 km, show more comparable statistical skill. Again, the subjective analysis of Figs. 4c and 4d indicated that the 1.3-km domain can still better resolve the small-scale valleys and ridges and better match the detailed wind observations. The same statistical result is generally true for the surface temperature errors in Fig. 6 where the finer resolution domains have smaller errors, and the 1.3-km domain has only a

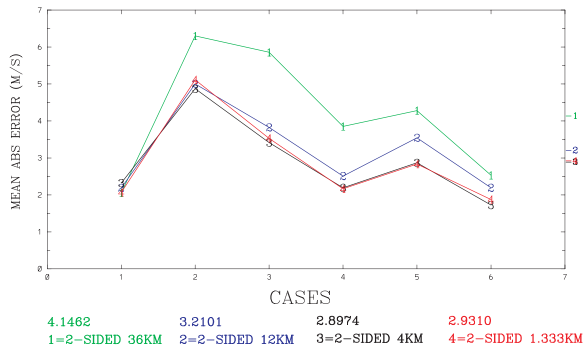

Figure 5. Mean absolute error of surface vector wind difference (ms^{-1}) for all four resolution model domains averaged over the 24-h forecast periods for all six cases over the 1.3-km domain area. Case-averaged values are plotted on right side of figure with numerical values in the experiment key.

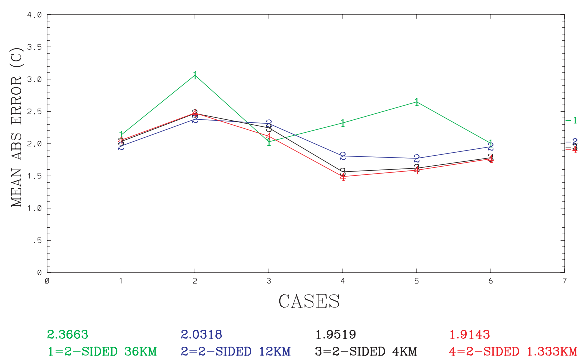

Figure 6. Mean absolute error of surface temperature (C) for all four resolution model domains averaged over the 24-h forecast periods for all six cases over the 1.3-km domain area. Case-averaged values are plotted on right side of figure with numerical values in the experiment key.

slight advantage over the 4-km domain case-averaged statistics.

Figure 7 shows the six-case-averaged vertical profiles of MAE for VWD for the 2-sided FDDA experiments. The higher resolution domains have smaller errors at the surface and in ABL while towards the top of the profile the coarser resolution model domains have smaller errors. The latter may be due to the relative decline in influence of terrain with altitude, while opportunity for contamination due to close-proximity artificial lateral boundaries grows for each successive nested domain. The case-averaged vertical profile of MAE temperature in Fig. 8 also shows better skill in lower levels with the higher resolution domains, and better skill in upper levels with coarser resolution domains. This grid resolution dependence in the statistical results is very

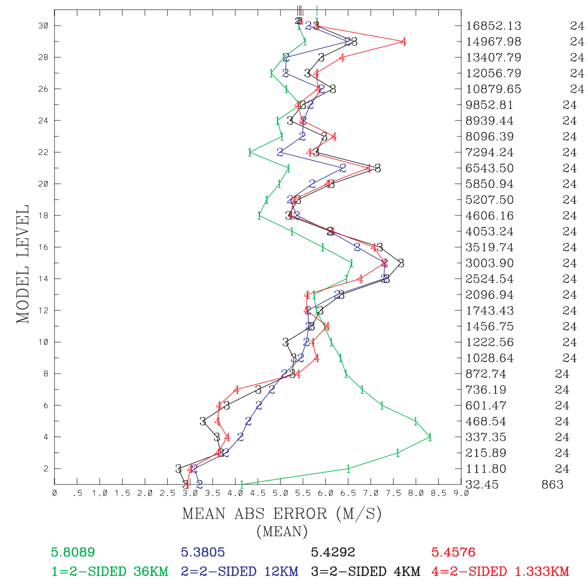

Figure 7. Profile of mean absolute error of vector wind difference (ms^{-1}) for the 2-sided FDDA experiment averaged over the 24-h forecast period for all six cases and the 1.3-km domain area for each of the four domains. Vertical averages are plotted at top of figure with numerical values given in the experiment key.

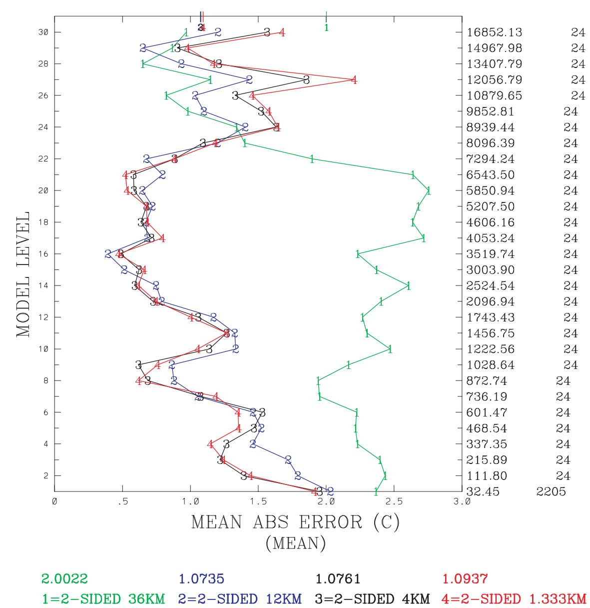

Figure 8. Profile of mean absolute error of temperature (C) for the 2-sided FDDA experiment averaged over the 24-h forecast period and all six cases for the 1.3-km domain area for each of the four domains. Vertical averages are plotted at top of figure with numerical values given in the experiment key.

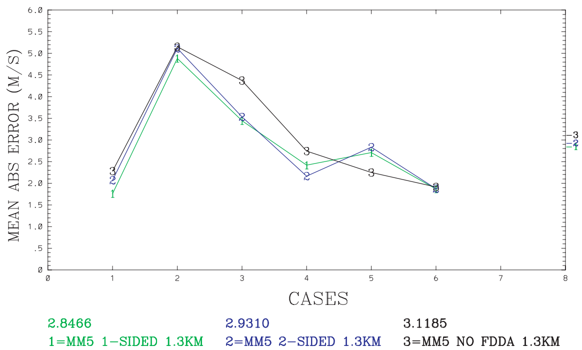

Figure 9. Mean absolute error of surface vector wind difference (ms^{-1}) averaged over the 24-h forecast period for the two FDDA experiments and no-FDDA experiment for each of the six cases on 1.3-km domain.

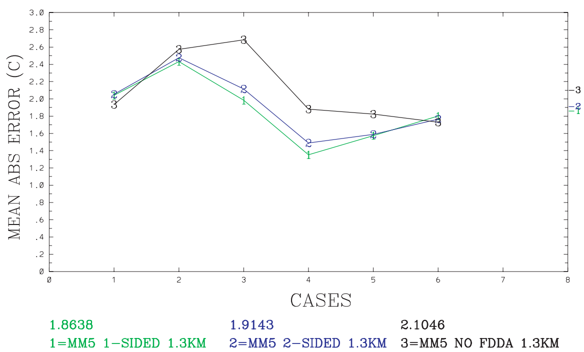

Figure 10. Mean absolute error of surface temperature (C) averaged over the 24-h forecast period for the two FDDA experiments and no-FDDA experiment for each of the six cases on 1.3-km domain.

similar to that for the 1-sided FDDA experiment and the no-FDDA experiment (not shown).

The effect of the pre-forecast running start FDDA period from the 1-sided and 2-sided FDDA experiments on the 1.3-km domain averaged MAE VWD and temperature over the 24-h forecast period at the surface for all six experiments is shown in Figs 9 and 10, respectively. The two FDDA experiments have generally comparable forecast error values with both being lower than that of the no-FDDA experiments over the six cases for both surface mass and wind fields. The vertical profiles in Figs. 11 and 12 again show consistent added value of FDDA, with 2-sided FDDA verifying slightly better than 1-sided FDDA on average, for the subsequent 24-h averaged forecasts of winds and temperature.

The MET fields for Case 5, representing the smallest impact of model FDDA on surface wind forecasts in Fig. 9, are used to drive HPAC predictions. The difference in impact of FDDA may

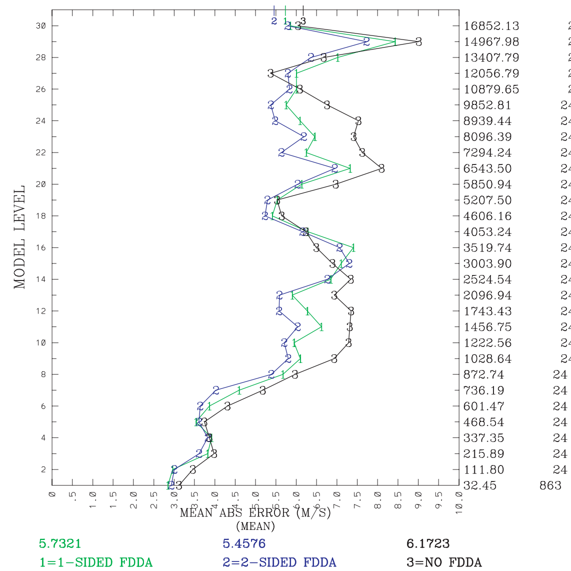

Figure 11. Profile of mean absolute error of vector wind difference (ms^{-1}) for the 24-h forecast period for two FDDA experiments and the no-FDDA experiment averaged over all six case days on the 1.3 km domain. Vertical averages are plotted at top of figure with numerical values given in the experiment key.

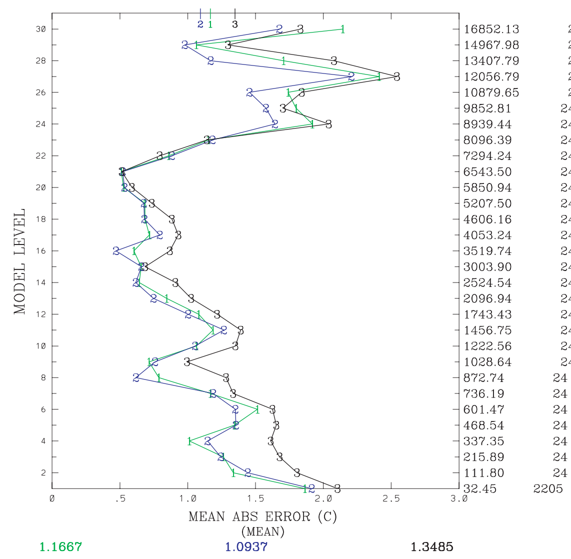

Figure 12. Profile of mean absolute error of temperature (C) for the 24-h forecast period for two FDDA experiments and the no-FDDA experiment averaged over all six case days on the 1.3 km domain. Vertical averages are plotted at top of figure with numerical values given in the experiment key.

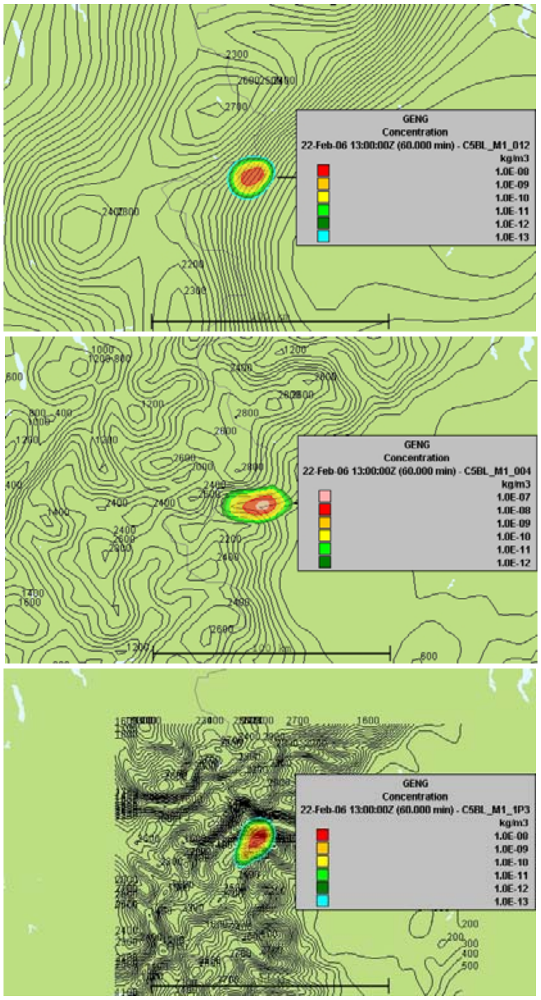

Figure 13. HPAC/SCIPUFF 1-h plume predictions and model terrain from the no-FDDA forecasts valid at 13 UTC 22 February 2006 over the 1.3-km domain area. a) 12-km resolution, b) 4-km resolution, c) 1.3-km resolution

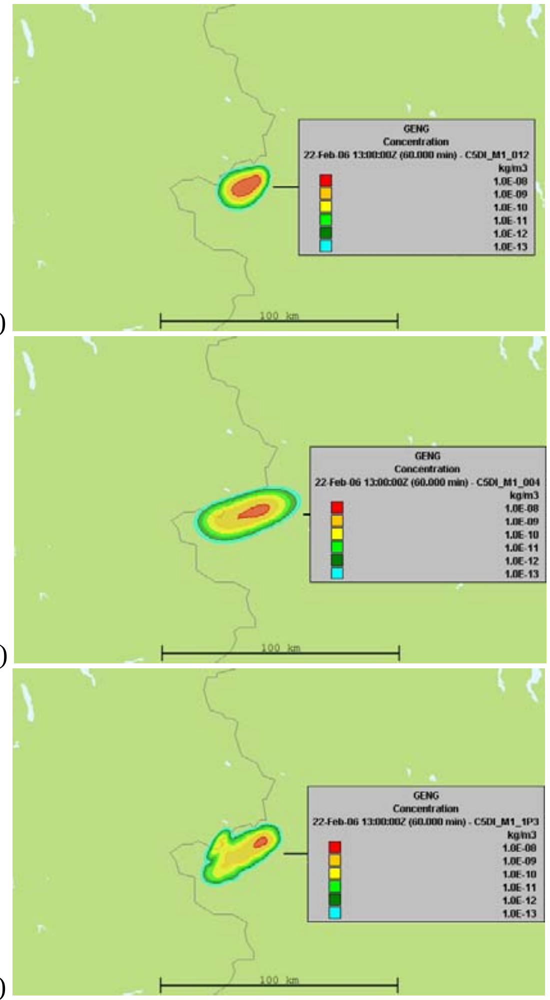

Figure 14. HPAC/SCIPUFF 1-h plume predictions and model terrain from the running-start FDDA forecasts valid at 13 UTC 22 February 2006 over the 1.3-km domain area. a) 12-km resolution, b) 4-km resolution, c) 1.3-km resolution

be due to Case 5 having somewhat fewer sondes and surface observations in the pre-forecast period and the forecast verification period than the other cases. Some HPAC results such as those in Fig. 13 will be presented at the conference for hypothetical releases in the mountains and on the plains using different MET inputs from Case 5. Although the MET statistical differences between the finer resolution grids may appear quite small (e.g., Figs. 5 and 6), hypothetical mountain releases and their 1-h HPAC plume predictions shown in Fig. 13 over the same 1.3-km domain area using the no-FDDA 12-km, 4-km and 1.3-km MET datasets suggest that this may not be the case for AT&D. Note that the shape and orientation of these plumes are distinctly different and that the 1.3-km HPAC prediction is most consistent with the dynamic-analysis northeasterly wind fields during this period (not shown). Figure 14 indicates that these HPAC predicted plumes based on the same 12-km, 4-km and 1.3-km resolution MET predictions but using the running-start FDDA are all oriented northeast-southwest, which is consistent with the dynamic analysis winds (not shown). Furthermore, the 1.3-km HPAC prediction indicates an appendage in the plume towards an adjacent ridge to the northwest, perhaps reflecting the impact of its higher resolution terrain. Thus, use of FDDA and finer model resolution also appears to produce more reasonable plume predictions based on local terrain considerations and observed winds.

5. CONCLUSIONS

The meteorological model results for the six cases (Table 1) representing the range of weather conditions observed over the study region during the February 2006 winter Olympics period generally show improved predictive skill when using data assimilation and increasing model resolution, especially at the surface and in the boundary layer. The improvements appeared to be larger for the precipitation cases (Cases 2 – 5) than the dry or light precipitation cases (Cases 1 and 6). Statistical MET differences were relatively small between the 4-km and 1.3-km grids, although subjective analysis and HPAC plume predictions sometimes revealed greater mesoscale details using 1.3-km resolution. This poses important questions as to whether finer model resolution is warranted for AT&D applications: small statistical differences in high-resolution MET fields can produce large differences in the AT&D plume predictions.

6. ACKNOWLEDGMENTS

We acknowledge ARPA Piemonte and Massimo Milelli for providing us their special weather observation data. Laurie Carson of NCAR managed the observation exchange site with the Italians. Karen Tinklepaugh assisted in the preparation of this manuscript. This work was sponsored by DTRA through contract DTRA01-03-D-0013 with L3-Titan.

7. REFERENCES

Deng, A, N. L. Seaman, G. K. Hunter, and D. R. Stauffer, 2004: Evaluation of inter-regional transport using the MM5/SCIPUFF system. *J. Appl. Meteor.*, **43**, 1864-1886.

Deng, A., and D.R. Stauffer, 2006: On improving 4-km mesoscale model simulations. *J. Appl. Meteor.,* **45,** 361-381.

Grell, G., J. Dudhia and D.R. Stauffer, 1995: A description of the fifth-generation Penn State/NCAR mesoscale model (MM5). NCAR Tech. Note NCAR/TN-398+STR, 122 pp.

Schroeder, A.J., D.R. Stauffer, N.L. Seaman, A. Deng, A.M. Gibbs, G.K. Hunter, and G.S. Young, 2006: An automated high-resolution, rapidly relocatable meteorological nowcasting and prediction system. *Mon. Wea. Rev.,* **134,** 1237-1265.

Stauffer, D.R., G.K. Hunter, A. Deng, Y.C. Kwon, P. Hayes, J. Trigg, Jr., 2006: Penn State-DTRA high resolution meteorological modeling for the Torino Winter Olympics, WRF Users' Workshop, Boulder CO, June 21, 4 pp.

Stauffer, D.R. and N.L. Seaman, 1994: Multiscale four-dimensional data assimilation. *J. Appl. Meteor.,* **33**, 416-434.